



HAL
open science

Physico-chemical characterisation of plant particles with potential to produce biobased building materials

Santiago Arufe, Arthur Hellouin de Menibus, Nathalie Leblanc, H el ene Lenormand

► **To cite this version:**

Santiago Arufe, Arthur Hellouin de Menibus, Nathalie Leblanc, H el ene Lenormand. Physico-chemical characterisation of plant particles with potential to produce biobased building materials. *Industrial Crops and Products*, 2021, 171, pp.113901. 10.1016/j.indcrop.2021.113901 . hal-03383272

HAL Id: hal-03383272

<https://hal.science/hal-03383272>

Submitted on 22 Aug 2023

HAL is a multi-disciplinary open access archive for the deposit and dissemination of scientific research documents, whether they are published or not. The documents may come from teaching and research institutions in France or abroad, or from public or private research centers.

L'archive ouverte pluridisciplinaire **HAL**, est destin ee au d ep ot et  a la diffusion de documents scientifiques de niveau recherche, publi es ou non,  emanant des  tablissements d'enseignement et de recherche fran ais ou  trangers, des laboratoires publics ou priv es.



Distributed under a Creative Commons Attribution - NonCommercial 4.0 International License

1 **Physico-chemical characterisation of plant particles with potential to produce biobased**
2 **building materials**

3 **Santiago Arufe^{a*}, Arthur Hellouin de Menibus^{b,c}, Nathalie Leblanc^a, H el ene**

4 **Lenormand^a**

5 ^aUniLaSalle, Univ. Artois, ULR7519 - Transformations & Agro-ressources, Normandie

6 Universit e, F-76130 Mont Saint Aignan, France

7 ^bEco-Pertica, L'H otel Buissonnet, 61340 Noc e, France

8 ^cFrench National Association of Short Distribution Network Hemp Producers (Association

9 Nationale des Chanvriers en Circuits Courts), France

10

11 *Corresponding Author: santiago.arufe@gmail.com

12

13 **Abstract**

14 **A physico-chemical characterisation of flax shiv (*Linum usitatissimum*), hemp shiv (*Cannabis***
15 ***sativa* L.), maize bark (*Zea mays* L.), miscanthus (*Miscanthus*), reed (*Phragmites australis*),**
16 **rice husk (*Oryza sativa*), sunflower (*Helianthus annuus*) bark and pith and wheat (*Triticum***
17 **by means of chemical composition, particle size, density and water behaviour was carried out**
18 **in order to facilitate their comparison. Particle size distribution, water sorption isotherms and**
19 **water absorption kinetics of the plant particles were modelled using respectively the log-**
20 **normal distribution, GAB and Nagy and Vas models. Results of chemical composition**
21 **(soluble compounds 6.0-38.6 g/100 g dry material (% d.b.), hemicellulose: 5.0-34.8 % d.b.,**
22 **cellulose: 23.3-49.0 % d.b., lignin: 3.3-41.7 % d.b., ashes: 2.4-13.7 % d.b.) highlight the**
23 **heterogeneity of the studied materials. Sunflower bark showed the largest mean values for**
24 **length (10.7 mm) and width (3.9 mm) hemp shiv being the smallest studied particle with 4.5**
25 **mm of length and 1.2 mm of width. The range of values of bulk density for the studied**
26 **samples varied from 21 kg/m³ (sunflower pith) up to 157 kg/m³ (sunflower bark). A slight**
27 **linear relationship ($R^2 < 0.87$) was found between porosity and bulk density of plant particles.**

28 Water absorption kinetics were consistent with the plant chemical composition and the open
29 porosity which highlight a fair understanding of inter-dependence of particles physical
30 properties.

31 **Keywords:** density; porosity; sorption; bio-based aggregate; building material

32

33 **1. Introduction**

34 The renovation and construction of buildings reducing the global warming potential can be
35 partly addressed by using low-environmental-impact materials such as raw biobased
36 materials. **In France**, hemp and straw are the most well-known plants used for building
37 applications (Colinart et al., 2020), hemp crop represented 17000 ha in 2018 (FAOSTAT) and
38 it generated about 50000 t of hemp shiv. Hemp production can be increased due to its
39 usefulness for farmers that goes toward low impact agriculture schemes. **A way to enhance**
40 **the sustainability could be diversify the use of different biobased particles in construction**
41 **rather than the use of only one kind of plant particle. Firstly, this may allow the use of plant**
42 **particles available at local scale. Secondly, it could reduce the risk of competition with other**
43 **ways for the valorisation of the same plant particles (litter, bioenergy, etc).** Laborel et al.
44 (2016) **in their review about earth construction** highlighted the great diversity of bio-
45 aggregates (plant and animal) **used** worldwide. This review identified cereal straws (wheat,
46 barley, oat, lavender (Giroudon et al., 2019)), wood aggregates (shavings or fibres), bast
47 fibres (hemp, flax, jute, kenaf, diss), palm tree fibres (coir, palm, date), wastes and residues
48 (cassava, millet, cotton, tea, tobacco, grass), leaf fibres (sisal, banana, pineapple), aquatic
49 plants (phragmite, typha, seaweed) and wool (sheep). **Jiang et al. (2020) specifically**
50 **characterized hemp shiv, flax shiv, rape shiv and wheat straw as hygric and insulating**
51 **construction materials for energy efficient building. Other works assessed the use of maize or**
52 **sunflower bark chips (Lagouin et al., 2019), reed (Honoré et al., 2020), miscanthus**
53 **(Ntimugura et al., 2020) and rice/rice husk ash (Taye et al., 2021) for bio-based building**
54 **materials.** In France, the **main** crops able to produce particles with potential applications in

55 construction are cereals (wheat, barley, oat, rye, rice), oil plants (sunflower, rapeseed),
56 herbaceous plants (corn, miscanthus, reed) and fibre plants (flax, hemp).

57 Microstructure and biochemistry are **two of the important parameters** to be studied in order to
58 understand how plant particles would behave when used as a building material. The
59 microstructure of plant particles can be studied at different scales (Glé et al., 2021). The bulk
60 density, **which is characterized by the mass of the particles per volume unit**, gives the overall
61 density of the bulk plant material. It is calculated by measuring the **total** volume occupied by a
62 certain mass of plant particles. **The total volume is the result of the sum of different volumes:**
63 **a) the volume occupied by the walls of the particles; b) the volume of air between the particles**
64 **and c) the volume of occupied air inside the particles.** The volume occupied by the walls of
65 **the particles (a) could be considered intrinsic of the material.** The air-filled volume between
66 **the particles (b) is dependent on the arrangement of the particles between them which is**
67 **influenced by their shape and particle size.** Therefore, this volume may be decreased by
68 **grinding or milling which could have a positive effect on the arrangement between the**
69 **particles and as a consequence increase the apparent density.** Finally, c) includes the volume
70 **accessible from the outside of the particle (open porosity) and the volume not accessible**
71 **(closed porosity) (Delannoy et al., 2020).**

72 **Functionalities are properties induced by the intrinsic characteristics of plant particles.** These
73 **characteristics such as the microstructure, chemical composition or water behaviour may lead**
74 **to functionalities that can be positive or negative depending on the final use of the plant**
75 **particle.** A clear example of a functionality related to chemical composition that can be
76 **positive or negative as function of the final use is the search for ecological solutions in the**
77 **design of particleboard.** By using the self-adhesion capacity, it is possible to process particle
78 **boards without the addition of binders, thanks to the action of different parameters such as**
79 **solubilization of molecules, temperature and pressure which allow the particles to**
80 **agglomerate with each other (Lenormand et al., 2017, Pintiaux et al., 2015).** However, this
81 **ability to solubilize molecules could be considered a negative functionality when the**

82 molecules disturb the setting of lime or cement-based mortars (Diquélou et al., 2015; Wang et
83 al., 2019).

84 The cell walls of plant particles are mainly composed of a mix of organic macromolecules
85 (pectins, cellulose, hemicelluloses, lignin, waxes, starch, proteins, aromatic compounds, **short-**
86 **chain sugars**) and a minority of mineral molecules such as ashes. Cell walls can therefore be
87 considered as biochemically complex composites. Cellulose molecules, hemicelluloses and
88 pectins are polysaccharides (polymers of carbohydrates) with hydrophilic **properties**. The
89 water-soluble compounds generally correspond to pectins and **short-chained** soluble
90 molecules. The proportions of organic macromolecules vary according to the botanical
91 species and the location in the plant. For example, sunflower pith stands out from the others
92 with a proportion of water-soluble compounds **higher** than 50% (Chabriac et al., 2016).

93 In order to clear out what are the essential differences between these plant particles, **a**
94 **physico-chemical characterization with the same techniques and protocols in order to**
95 **facilitate the comparison was carried out**. The procedure was applied to 9 different plant
96 particles **that** can be obtained in France, focusing on the particle size, the hygroscopic
97 behaviour, the chemical composition, the densities and the water absorption behaviour.

98

99 **2. Materials and Methods**

100 **2.1. Materials**

101 Nine different plant particles were studied: **A)** flax (*Linum usitatissimum*) shiv bought on a
102 local market, Linabox (76590 Crosville sur Scie, France); **B)** hemp (*Cannabis sativa L.*) shiv
103 bought in a local market and produced in France; **C)** maize (*Zea mays L.*) bark particles
104 obtained from stems of maize cultivated in Villainville (Seine-Maritime, France) in 2015; **D)**
105 miscanthus (*Miscanthus*) particles obtained on a local market, Miscanplus (28250 Digny,
106 France); **E)** reed (*Phragmites australis*) particles obtained after milling and sieving (the
107 studied fraction corresponded to particles that were retained between 2 and 8 mm sieves) of
108 reed from the Brenne region (Centre-Val de Loire, France); **F)** rice (*Oryza sativa*) husk,

109 obtained from a high density batch (Balle Concept, 13200 Arles, France) that was sieved with
110 a sieve of 10 mm, vacuuming once to remove heavy parts (grains and others) and re-sieved
111 with a sieve of 10 mm; **G**) sunflower (*Helianthus annuus*) bark and sunflower pith (**H**)
112 obtained from sunflower stem kindly provided by the farm cooperative *Oxyane* and **I**) wheat
113 (*Triticum*) particles obtained from wheat cultivated in Normandie in 2017.
114 The employed hemp and flax shiv were obtained by raw plant transformation by a large scale
115 defibrator plant that was hammer milled during the defibrating process. Maize bark and wheat
116 studied particles were obtained after milling employing a cutting mill (Retsch SM100,
117 Germany) equipped with a standard sieve with 10 mm of mesh size. All different samples
118 were sieved employing a standard sieve of 0.5 mm in order to eliminate dust that could have
119 influence on the subsequent studies.

120 *Location of Figure 1*

121

122 **2.2. Chemical Composition**

123 Chemical composition of samples, content of ash, lignin, cellulose, hemicellulose and soluble
124 **compounds** in neutral detergent was determined following the Van Soest method (AFNOR,
125 1997, Viel et al., 2018) employing an adapted machine (FibertcTR 8000, Foss, Denmark). To
126 carry out this measurement all samples were previously dried until constant weight at **40°C**
127 **using an oven (Memmert, Germany)** and then milled employing a micro impact mill (Culatti,
128 Switzerland), the rotor speed was adjusted to 7 and a standard sieve of 1 mm of mesh size was
129 employed. All measurements were carried out at least in triplicate.

130

131 **2.3. Particle size characterization**

132 Particle size distribution of all samples was determined by image analysis employing the
133 protocol described by Amziane & Collet (2017) slightly modified. Images of each sample
134 were taken employing a vision system (Keyence, CA-MX500M) placing their particles on a
135 plate (CA-DSW15) where a maximum of 200 particles were placed to take the photos. Size of

136 particles was then determined employing a scale factor of 0.0609 mm/pixel employing the
137 associated software of the machine. At least 1000 particles of each sample were measured.
138 Experimental data was modelled employing the error function in order to confirm if this
139 function can be a good model to predict experimental particle size distribution of samples.
140 The model is defined as, Eq. (1):

141

$$142 \quad P = \frac{1}{2} \left(1 + \operatorname{erf} \left(\frac{\ln(x) - \mu}{\sqrt{2}\sigma} \right) \right) \quad (1)$$

143

144 where P is the cumulative frequency, erf the error function ($\operatorname{erf}(z) = \frac{2}{\sqrt{\pi}} \int_0^z e^{-t^2} dt$), x the
145 variable (in this case width or length) and μ and σ are model parameters corresponding to
146 mean and standard deviation of the variable's natural logarithm.

147

148 **2.4. Bulk and true density**

149 **2.4.1. Bulk Density**

150 Two different bulk densities of samples previously dried at 40°C until constant weight were
151 calculated employing different methods: apparent and compacted density. Apparent density
152 (ρ_A) was calculated by measuring the height of a known quantity of sample placed in a
153 cylinder that was upended ten times (Amziane & Collet 2017). For compacted density (ρ_C) a
154 known quantity of samples was placed in a cylinder then it was manually compressed and
155 finally the volume of the sample was determined (Glé et al., 2021). All measurements were
156 carried out at least in triplicate.

157

158 **2.4.2. True Density**

159 True density (ρ_T) of samples was calculated after measurement of sample volume by gas
160 displacement using a gas pycnometer (Pycnomatic Evo, ThermoScientific) with argon as
161 employed gas. The gas was introduced into a small vessel (21.42 cm³) at a constant
162 temperature of 23°C where the sample was previously placed. The pressure (P) was set at 1

163 bar (with highest and lowest limit of 1.5 bar and 0.5 bar, respectively) considering that sample
164 is in equilibrium when ΔP between different measurements is lower than 0.00020 bar and
165 volume standard deviation lower than 0.050 %. True density was then calculated by ratio of
166 sample mass (previously determined) and sample volume determined by gas displacement.
167 Each sample was measured at least in duplicate.

168 Once both true and apparent density were obtained, open porosity was calculated as follows,
169 Eq. (2):

170

$$171 \theta_{open} = 1 - \frac{\rho_A}{\rho_T} \quad (2)$$

172

173 where θ_{open} corresponded to open porosity (-) and ρ_A and ρ_T to, respectively, apparent and true
174 density (kg/m^3) of samples determined as previously explained.

175

176 **2.5. Water sorption isotherms**

177 Water sorption isotherms of samples were determined at 23°C using a Dynamic Vapour
178 Sorption machine (SPS-Sorption Test System, proUmid), employing nitrogen as gas in order
179 to control relative humidity (φ). At least duplicate samples (219 ± 34 mg as average sample
180 weight) were measured. Different equilibrium points were determined corresponding to a
181 fixed relative humidity: 0, 5, 10, 15, 20, 30, 35, 50, 75, 85 and 90 % for adsorption
182 experiments, and 0, 15, 30, 35, 50, 75, 85, 90 % for desorption experiments. Samples
183 employed for adsorption experiments were previously air-dried until constant weight in an
184 oven (Mettler, Germany) at 40°C. Desorption samples were previously exposed to a relative
185 humidity of 90% for hydration until they reached a constant weight.

186 **GAB** (van den Berg & Bruin (1981), Eq. (3)) and BET models (Brunauer *et al.*, 1938, Eq. (4))
187 were employed to model water sorption experimental data (equilibrium moisture content, X_{eq}
188 versus φ):

189

$$190 \quad X_{eq} = \frac{X_m K C \phi}{(1-K\phi)(1-K\phi+CK\phi)} \quad (3)$$

191

$$192 \quad X_{eq} = \frac{X_m C \phi}{(1-\phi)(1+(C-1)\phi)} \quad (4)$$

193

194 where X_m is the monolayer moisture content (kg water/kg dried solid, **dry basis: d.b.**), C
 195 (dimensionless, -) and K (dimensionless, -) is a parameter related to the heat of sorption of the
 196 multilayer in GAB model. The values of GAB model parameters give different information. C
 197 parameter is related to the water bound in the monolayer, the higher C , the stronger water is
 198 bound in the monolayer and the higher the difference in enthalpy between the monolayer
 199 molecules and multilayer molecules (Quirijns et al., 2015). K is called a correction factor,
 200 since it corrects the properties of the multilayer molecules relative to the bulk liquid. When K
 201 approaches one, there is almost no distinction between multilayer molecules and liquid
 202 molecules. In that case the water molecules beyond the monolayer are not structured in a
 203 multilayer, but have the same characteristics as the molecules in the bulk liquid. The more the
 204 sorbed molecules are structured in a multilayer, the lower the value for K (Quirijns et al.,
 205 2015). Finally, X_m is a measure of the availability of active sites for water sorption by the
 206 material. It has to be noted that BET was applied in the range of relative humidity from 0.05
 207 to 0.35 in order to determine the specific surface area of samples (**Collet et al., (2008)**)
 208 assuming that X_m of BET model represents the quantity of water molecules that covers the
 209 entire surface as a monolayer and no diffusion of water through the material **has** taken place.
 210 Experimental data was modelled using these two methods employing Solver function of Excel
 211 software. In the case of BET model, once model parameters were obtained, specific surface
 212 area was calculated as follows, Eq. (5):

213

$$214 \quad a_s = \frac{X_m L a_m}{M_w} \quad (5)$$

215

216 where a_s is the specific surface area of the sample (m^2/g), L the Avogadro constant ($6.023 \cdot 10^$
217 $^{23} \text{mol}^{-1}$), a_m cross sectional area of water molecule ($1.08 \cdot 10^{-19} \text{m}^2$) and M_w molecular weight
218 of water molecules (18g/mol).

219

220 **2.6. Water absorption kinetics**

221 Water absorption kinetics of different samples were determined at 5, 15, 60, 480, 1440, 2880
222 min (t) employing a protocol based on the one previously published by Amziane & Collet
223 (2017) with some modifications. Samples ($M_0 \approx 1 \text{g}$) previously dried at 40°C until constant
224 weight using an oven (Memmert, Germany) were put in a water bath (water temperature
225 $23.0 \pm 0.5^\circ\text{C}$) during different periods of time employing a tea strainer ball. Once the desired
226 time of immersion was achieved, samples were removed and filtered by vacuum filtration
227 with a Büchner funnel using a paper filter, in order to eliminate the excess of water on the
228 surface of the material, and finally weighed to determine the mass of the sample after
229 immersion (M_t , g). Afterwards, samples were dried in an oven (Memmert, Germany) at 105°C
230 until constant weight ($M_{105^\circ\text{C}}$, g). Each experimental data point of water absorption kinetics
231 were carried out at least in triplicate.

232 In order to analyse the water absorption kinetics different parameters were calculated: water
233 absorption related to initial dry mass (WA_{M_0} , kg water/kg initial dry mass, Eq. (6)); water
234 absorption related to final dry mass (WA_{M_f} , kg water/kg final dry mass, Eq. (7), which takes
235 into account the mass lost due to leaching during immersion) and solid loss during immersion
236 (SL , kg lost dry solid/kg final dry mass, Eq. (8)):

237

$$238 \quad WA_{M_0} = \frac{M_t}{M_0} \quad (6)$$

239

$$240 \quad WA_{M_f} = \frac{M_t}{M_{105^\circ\text{C}}} \quad (7)$$

241

$$242 \quad SL = \frac{M_0 - M_{105^\circ\text{C}}}{M_{105^\circ\text{C}}} \quad (8)$$

243

244 These parameters were finally modelled employing a function developed by Nagy and Vas
245 (Nagy and Vas 2003) that gives an asymptotically correct approximation of the capillary
246 water uptake process for both $t \rightarrow 0$ and $t \rightarrow \infty$, Eq. (9):

247

$$248 \quad \Delta m(t) = \Delta m_{\infty} (1 - e^{-At^{\frac{1}{2}B}})^B \quad (9)$$

249

250 where A and B are constant parameters, Δm_{∞} is the modelled parameter related to equilibrium
251 (when $t \rightarrow \infty$) and $\Delta m(t)$ is the experimental data of water absorption kinetics (W_{AM0} , W_{AMF}
252 or SL).

253

254 **2.7. Scanning electro microscopy (SEM)**

255 Images of samples were taken employing scanning electro microscopy (JSM-IT100 LA,
256 JEOL, Japan) under vacuum conditions (40 Pa) and an accelerating voltage of 15 kV.

257

258 **2.8. Statistical analysis**

259 The goodness of the adjustment of each model was determined based on coefficient of
260 determination (R^2) and root mean square error (E_{RMS} , Eq. (10)):

261

$$262 \quad E_{RMS} = \left[\frac{1}{N} \sum_{i=1}^N (X_{exp} - X_{cal})^2 \right]^{1/2} \quad (10)$$

263

264 where N is the number of data points, X_{exp} the experimental data point and X_{cal} the calculated
265 data point using the corresponding model. The values of the parameters of each model were
266 obtained with an automated least square minimization approach.

267

268 **3. Results and Discussion**

269 3.1. Chemical Composition

270 Table 1 highlights the heterogeneity of the studied materials. In the case of soluble
271 compounds, the range values varied from 6.0 up to 38.6 % d.b., sunflower pith had the highest
272 value whereas sunflower bark presented the lowest one. Most of the studied samples
273 presented values of soluble compounds around 10 % d.b.. Hemicellulose ranged between 5.0
274 to 34.8 % d.b and in most of the studied samples it was the second most important fraction on
275 the materials composition. Cellulose is the main component of all studied samples except for
276 sunflower bark and pith where the highest percentage corresponded respectively to lignin and
277 soluble compounds. The cellulose values varied from 23.3 to 49.0 % d.b.. Lignin represented
278 between 3.3 to 41.7 % d.b.. Finally, ashes varied from 2.4 % for miscanthus to 13.7 % d.b. for
279 rice husk. Except for sunflower pith and rice husk, the percentage of ashes on the studied
280 samples always represented the smallest part of their composition.

281 The composition of the different studied plant particles was similar of the one previously
282 published in literature by different authors even if in certain cases the comparison is difficult
283 due to the use of different methods. Flax shiv (Mahieu et al., 2019), hemp shiv (Viel et al.,
284 2018), maize bark (Zhang et al., 2018), miscanthus (Ntimugura et al., 2020), reed (Honoré et
285 al., 2020), rice husk (Chandrasekhar et al., 2003), sunflower bark and pith (Chabriac et al.,
286 2016) and wheat (Viel et al., 2018).

287 For a specific plant, its chemical composition may vary as function of the geography, the
288 weather and the maturity of the plant (Viel et al., 2018). The botanical species and the
289 location in the plant can also influence the chemical composition. In this sense, the difference
290 on chemical composition between sunflower bark and pith could be explained by their
291 location. Sunflower bark, which is obtained from outer part of the stem (mainly responsible of
292 the structural stability of the plant), had a higher proportion of hemicellulose, cellulose and
293 lignin because they are polymers with a very important supportive structural function. On the
294 other hand sunflower pith, obtained from the inner part of the stem where the structural
295 function is less important, presented a lower proportion of these polymers and a higher

296 proportion of non-structural components (soluble compounds). Hemp and flax shiv show
297 similar compositions (mainly composed of cellulose), which may also be linked to the fact
298 that they are obtained from the same location of the plant stem. Chemical composition of
299 wheat particles and maize bark particles are similar, with high contents of hemicellulose and
300 cellulose, and intermediate contents of soluble compounds. For miscanthus and reed particles
301 chemical composition is similar, with high contents of hemicellulose and cellulose, and low
302 contents of soluble compounds. Compositions of sunflower pith, sunflower bark and rice husk
303 particles differ from all others with, respectively, high content of soluble, lignin and ash.

304

305 *Location of Table 1*

306

307 **3.2. Particle size characterization, density and porosity**

308 Particle size characterization of different samples showed that most of them can be
309 satisfactorily fitted employing a lognormal model for both length and width parameters
310 ($R^2 > 0.993$ and $E_{RMS} < 0.027$). The exception corresponded to rice husk length where the
311 lognormal model was unable to fit rice husk length, particularly at lower sizes, Table 2.
312 Taking into account that the selected plant particles may come from different parts of the
313 plant: 1) the inner part of the stem (flax shiv, hemp shiv, sunflower and maize pith); 2) the
314 outer part of the stem (sunflower and maize bark); 3) the whole stem (fragments of the stems
315 obtained after grinding: wheat or miscanthus) or 4) the husks (envelopes) of grains of rice and
316 the differences in terms of shape and texture could be remarkable, from elongated and rigid
317 (i.e. sunflower bark, miscanthus) to thin and deformable (i.e. flax shiv, wheat or reed) or
318 spherical/cubic and sponge-like (i.e. sunflower pith particles) the use of the same model to
319 manage their particle size distribution may prove to be useful. Largest and smallest particles
320 for both length and width were the same: sunflower bark showed the largest mean values
321 (10.7 mm for length and 3.9 for width) hemp shiv being the smallest studied particle with a
322 mean value of 4.5 mm for length and 1.2 mm for width. Several particles were ground up

323 and/or sieved during the transformation process, so the particle size distribution is not an
324 intrinsic property of plant particles.
325 Regarding density values, it has been found that in the case of bulk density sunflower bark
326 showed the highest value followed by miscanthus, hemp shiv, rice husk and flax shiv, Table
327 2. The lowest values corresponded to sunflower pith, wheat, maize bark and reed. The range
328 of values for the studied samples varied between 21 kg/m^3 and 157 kg/m^3 , which is the result
329 of differences between intrinsic properties of each material and of the grinding and/or sieving
330 process. These values are in accordance with those previously published by Chabriac et al.
331 (2016), which studied hemp shiv, sunflower bark and pith, flax shiv and rapeseed.

332 *Location of Table 2*

333

334 In the case of true density, sunflower pith was also the material with the lowest density.
335 However, it was observed that for the other studied samples, true density did not follow the
336 same trend of bulk density. For example, flax shiv and sunflower bark presented the highest
337 true density whereas they showed intermediate bulk densities. This fact reflects that bulk
338 density can be influenced by other properties of the material such as particle size and shape
339 that could lead to different arrangement of the material in the bulk. Specifically, in the case of
340 sunflower bark this difference can be related to the higher particle size in the bulk which
341 could lead to an arrangement in the bulk with higher void volume leading to a lower bulk
342 density. In this sense, this is corroborated by the higher porosity obtained for this material.
343 Even if grinding and sieving processes affect the particle shape and arrangement, a slight
344 linear relationship ($R^2 < 0.87$) between the porosity and the bulk density was found: the higher
345 the porosity, the lower the bulk density. Figure 1, shows as a qualitative example, the different
346 microstructures of each plant particle obtained employing SEM.

347

348 **3.3. Water sorption isotherms**

349 Water adsorption-desorption isotherms of all studied samples were satisfactorily modelled
350 employing GAB model (Eq. 3) ($R^2 > 0.9994$; $E_{RMS} < 0.003$; Table 3) which confirms the type II
351 isotherm (Collet et al., 2008), Figure 2a and 2b.

352 *Location of Table 3 and Figure 2*

353

354 At high relative humidities (>0.80), three main groups of plant particles could be established.
355 Sunflower pith, maize bark and hemp shiv presented equilibrium moisture contents >0.24 kg
356 water/kg initial dry solid; wheat and sunflower bark showed X_{eq} between 0.20 and 0.22 and
357 rice husk, miscanthus, reed and flax shiv were the ones with lower values (0.16-0.18 kg
358 water/kg initial dry solid). In the case of adsorption process, hemp shiv was the sample with a
359 stronger water bound in the monolayer followed by flax shiv and wheat whilst miscanthus and
360 sunflower bark were the samples with the weaker water bound. Regarding X_m , it has been
361 noticed that sunflower (bark and pith) had the higher values indicating a higher availability of
362 active sites for water adsorption being hemp shiv, wheat and maize bark the ones with the
363 lower values. This trend was corroborated by a_s values obtained employing Eq. (5), Table 3.
364 This fact makes hemp shiv the sample with the lower quantity of available active sites of all
365 studied samples but, at the same time, the one with the stronger bounded water. Moreover, K
366 value was near to 1 which means that water molecules that are not present in the monolayer
367 have almost the same behaviour as liquid molecules.
368 During desorption process all equilibrium moisture contents were higher compared to
369 adsorption process for each sample. In general, the samples with lower values for adsorption
370 process remained the same in the case of desorption process. However, in the case of flax shiv
371 and miscanthus the X_m for desorption process were the highest between all samples. This fact
372 could be related to the compositions of these materials, Table 1, which presented the lower
373 values of ash content having, consequently, a higher proportion of other compounds that
374 could help to retain or absorb water.

375

376 **3.4. Water absorption kinetics**

377 Experimental data of water absorption kinetics of all studied samples presented a similar
378 behaviour, Figure 3a. At the beginning of the immersion (first 500 min) samples quickly
379 absorb water and then an asymptotic process of water gain takes place until achieving the
380 equilibrium (48 h). A similar kinetic was the one observed for solid loss (SL) where it was
381 observed that the main SL during immersion takes place at the beginning of the immersion
382 process, Figure 3b. This phenomenon explains the difference between WA_{M0} and WA_{MF}
383 kinetics. As it can be observed, at the beginning of the immersion process samples absorbed
384 water and leach water-soluble compounds that lead to an increasing difference between WA_{M0}
385 and WA_{MF} . Once the equilibrium of SL is achieved and the leaching of soluble compounds
386 becomes almost negligible the difference between WA_{M0} and WA_{MF} remains constant.
387 Experimental data was satisfactorily modelled employing Nagy and Vas model, Eq. (9) for
388 WA parameters ($R^2 > 0.98$). In the case of SL modelling the fitting was not satisfactory
389 ($R^2 > 0.83$), Table 4.

390 *Location of Table 4 and Figure 3a and 3b*

391

392 Results revealed that sunflower pith was the sample with the highest water absorption
393 capacity (35.8 kg water/kg final dry solid) far higher than the other studied samples. The
394 range of values for the other studied samples varied from 2.3 for rice husk up to 7.1 (kg
395 water/kg final dry solid) for maize bark. Moreover, sunflower pith and rice husk were the
396 samples with a higher absorption rate (they reach the equilibrium water absorption capacity
397 faster than other ones), being hemp shiv, miscanthus and sunflower pith the ones with the
398 lower water absorption rate. This behaviour could be related to both chemical composition
399 and porosity of bulk material. In the case of hemp shiv and miscanthus they all have the lower
400 values of open porosity which could lead to a slower water absorption process. This is not the
401 case of sunflower pith, the explanation in this case may be found with the higher content of
402 lignin and the lower content of other compounds known to be hydrophilic.

403 Finally, Nagy and Vas model parameters related to equilibrium (SL_{∞}) were in accordance
404 with the trend obtained by Van Soest method for soluble compounds. However, their values
405 were systematically lower than those obtained by the Van Soest method. It can be explained
406 by the fact that during water absorption experiments only water-soluble compounds are
407 leaching from the sample and consequently determined, compared to Van Soest method
408 where the most part of soluble compounds (not only water-soluble) are quantified. The solid
409 loss may be related mainly to soluble compounds that are eliminated from the samples during
410 immersion.

411

412 4. Conclusions

413 Nine biobased particles available on French territory with an actual or potential use in
414 construction were studied. Their microstructure, densities, water behaviour and chemical
415 composition was compared. The novelty of this study lies in three essential contributions.
416 Firstly, all plant particles were characterized with exactly the same procedure and operator,
417 which allows a fair comparison between them in order to clear out their differences. Secondly,
418 results of particle size distribution (log-normal distribution model), water sorption isotherms
419 (GAB model) and water absorption kinetics (Nagy and Vas model) were satisfactorily
420 modelled using the same model for the different samples which could be useful for the
421 prediction or estimation of these properties for future applications. Finally, the water
422 absorption kinetics observed were found to be consistent with the chemical composition of the
423 plant particles and the open porosity, which highlight a fair understanding of inter-dependence
424 of particles physical properties.

425 Applications of the plant particle could be the use of the plant particle alone (i.e as a raw
426 insulation) or mixed with a binder such as clay (Colinart et al., 2020) or lime, to make
427 biobased concrete (light), wattle and daub (medium) or coating (heavy). Based on our results,
428 it can be concluded that there are no best or worst particles, but different particles with
429 varying degrees of difference depending on the studied property. The knowledge of such

430 differences between particles allows professional construction workers to select the best
431 particle for their need, or alternatively, to adapt its practices depending on the **plant** particle
432 locally available. For instance, quantity of **soluble compounds** might be an issue when using
433 lime binder. Water absorption rate **explains** the workability or texture evolution when the
434 particle is mixed with a binder in a mixer, or the hardening behaviour for sprayed biobased
435 concrete. Sorption in the medium relative humidity range **illustrates** the water regulation
436 capabilities of the material. **From a practical point of view it is useful to evaluate if the use of**
437 **a different plant particle in a biobased concrete would affect its water regulation capabilities.**
438 This study is a first step since it was carried out on only one batch for each type of plant.
439 Further studies might be focused on the variability of each plant types in order to assess the
440 range of dispersion for each studied characteristic. Plant diversity allows a wide range of
441 methods in construction. **Each construction applications (particle boards, lime-based**
442 **mortars/renders, earth-based mixes, etc.) has its own characteristics and interactions with**
443 **plant properties.** The multitude of specifications echoes the diversity offered by plants. By
444 working according to defined specifications, the diversity and complexity of plant particles
445 become a source of potential.

446

447 **CRedit authorship contribution statement**

448 Santiago Arufe: Conceptualization; Investigation; Validation; Writing original draft, review
449 and editing.

450 Arthur Hellouin de Ménibus: Conceptualization; Investigation; Validation; Writing review
451 and editing.

452 Nathalie Leblanc: Investigation; Validation; Writing review and editing.

453 H el ene Lenormand: Conceptualization; Investigation; Validation; Writing review and editing.

454

455 **Declaration of Competing Interest**

456 The authors report no declarations of interest.

457

458 **Acknowledgments**

459 The authors acknowledge the financial support of the Normandie region and FEDER for the
460 TIGRE research project, the Parc Naturel Régional du Perche (especially Florence Sbile),
461 Pierre Delot for kindly providing rice husk and several information regarding such plant
462 particles, Marianne Rosa and Jean Baptiste Besnier for additional measurements using SEM
463 and DVS.

464

465 **References**

- 466 AFNOR (1997). NF V 18-122-Aliments des animaux-Détermination séquentielle des
467 constituants pariétaux-Méthode par traitement aux détergents neutre et acide et à
468 l'acide sulfurique.
- 469 Amziane, S., Collet, F., 2017. Based Building Materials, Vol. 23 of RILEM State-of-the-Art
470 Reports, Springer Netherlands, Dordrecht.
- 471 Brunauer, S., Emmet, P.H., Teller E., 1938. Adsorption of gases in multimolecular layers. J.
472 Am. Chem. Soc. 60, 309-19.
- 473 Chabriac, P.A., Gourdon, E., Glé, P., Fabbri, A., Lenormand, H., 2016. Agricultural by-
474 products for building construction and modeling to predict micro-structural parameters.
475 Constr. Build. Mater. 112, 158-167.
- 476 **Chandrasekhar, S., Satyanarayana, K.G., Pramada, P.N., Raghavan, P., 2003. Review**
477 **Processing, properties and applications of reactive silica from rice husk-an overview. J.**
478 **Materials Sci. 38, 3159-3168.**
- 479 Colinart, T., Vincelas, T., Lenormand, H., Hellouin De Menibus, A., Hamard, E., Lecompte,
480 T., 2020. Hygrothermal properties of light-earth building materials. J. Build. Eng. 29,
481 101134.
- 482 Collet, F., Bart, M., Serres, L., Miriel., J., 2008. Porous structure and water vapour sorption of
483 hemp-based materials. Constr. Build. Mater. 22, 1271-1280.

484 Degrave-Lemeurs, M., Glé, P. Hellouin de Menibus, A., 2018. Acoustical properties of hemp
485 concretes for buildings thermal insulation: Application to clay and lime binders. *Constr.*
486 *Build. Mater.* 160, 462-474.

487 Delannoy, G., Marceau, S., Glé, P., Gourla. E, Guéguen-Minerbe, M., Diafi, D., Amziane, S.,
488 Farcas, F., 2020. Impact of hemp shiv extractives on hydration of Portland cement.
489 *Const. Buil. Mater.* 244, 118300.

490 Diquélou, Y., Gourlay, E., Arnaud, L., Kurek, B., 2015. Impact of hemp shiv on cement
491 setting and hardening: Influence of the extracted components from the aggregates and
492 study of the interfaces with the inorganic matrix. *Cem. Concr. Compos.* 55, 112-121.

493 Giroudon, M., Laborel-Préneron, A., Aubert, J. E., Magniont, C., 2019. Comparison of barley
494 and lavender straws as bioaggregates in earth bricks. *Constr. Build. Mater.* 202, 254-
495 265.

496 Glé P., Gourlay E., 2015. Rapport de recherche MABIONAT, Étude de l'influence de la
497 teneur en eau et du vieillissement sur les performances acoustiques et thermiques des
498 matériaux biosourcés.

499 Glé, P., Lecompte, T., Hellouin de Ménibus, A., Lenormand, H., Arufe, S., Château, C.,
500 Fierro, V., Celzard, A., 2021. Densities of hemp shiv for building: From multiscale
501 characterisation to application. *Ind. Crops Prod.* 164, 113390.

502 Honoré, M., Pimbert, S., Lecompte, T., 2020. Characterisation of plant flours for
503 biocomposite applications focussing on *Phragmites australis* properties. *Biosystems*
504 *Eng.* 197, 367-377.

505 Hussain, A., Calabria-Holley, J., Lawrence, M., Jiang, Y., 2019. Resilient hemp shiv
506 aggregates with engineered hygroscopic properties for the building industry. *Constr.*
507 *Build. Mater.* 212, 247-253.

508 Jiang, Y., Lawrence, M., Zhang, M., Cui J., 2020. Industrial bio-based plant aggregates as
509 hygric and insulating construction materials for energy efficient building. *Front. Chem.*
510 *Sci. Eng.*

511 Laborel-Preneron, A., Aubert, J, E. Magniont, C., Tribout, C., Bertron, A., 2016. Plant
512 aggregates and fibers in earth construction materials: A review. *Constr. Build. Mater.*
513 111, 719-734.

514 Lagouin, M., Magniont, C., Sénéchal, P., Moonen, P., Aubert, J.E., Laborel-Préneron, A.,
515 2019. Influence of types of binder and plant aggregates on hygrothermal and
516 mechanical properties of vegetal concretes. *Const. Build. Mater.* 222, 852-871.

517 Lenormand, H., Glé, P., Leblanc, N., 2017. Investigation of the acoustical and thermal
518 properties of sunflower particleboards. *Acta Acust united Ac.* 103, 149–157.

519 Mahieu, A., Alix, S., Leblanc, N., 2019. Properties of particleboards made of agricultural by-
520 products with a classical binder or self-bound. *Ind. Crops Prod.* 130. 371-379.

521 Nagy, V., Vas, L. M., 2003. Inrayarn Porosity and Pore Size in Polyester Staple Yarns. In:
522 International Textile Design and Engineering Conference Proceedings, Eninburgh,
523 United Kingdom, pp. 201-208.

524 Ntimugura, F., Vinai, R., Harper, A., Walker, P., 2020. Mechanical, thermal, hygroscopic and
525 acoustic properties of bio-aggregates – lime and alkali - activated insulating composite
526 materials: A review of current status and prospects for miscanthus as an innovative
527 resource in the South West of England. *Sustainable Mat. Tech.* 26, e00211.

528 Pintiaux, T., Viet, D., Vandenbossche, V., Rigal, L., and Rouilly, A. (2015). Binderless
529 materials obtained by thermo-compressive processing of lignocellulosic fibers: A
530 comprehensive review. *BioRes.* 10(1): 1915-1963.

531 Tayeh, B.A., Alyousef, R., Alabduljabbar, H., Alaskar, A., 2021. Recycling of rice husk waste
532 for a sustainable concrete: A critical review. *J. Cleaner Prod.* 312, 127734.

533 Quirijns, E.J., van Boxtel, A., van Loon, W., van Straten, G., 2005. Sorption isotherms, GAB
534 parameters and isosteric heat of sorption. *J. Sci. Food Agric.* 85:1805–1814.

535 van den Berg, C., Bruin, S., 1981. Water activity and its estimation in food systems:
536 theoretical aspects. In L. B. Rockland and G. F. Stewart (Eds.), pp. 1-61.

537 Viel, M., Collet, F., Lanos, C., 2018. Chemical and multi-physical characterization of agro-
538 resources' by-product as a possible raw building material. *Ind. Crops Prod.* 120, 214-
539 237.

540 Wang, L., Lenormand, H., Zmamou, H., Leblanc N., 2019. Effect of soluble components from
541 plant aggregates on the setting of the lime-based binder. *J. Renew. Mater.* 7, 9, 903-913.

542 Zhang, J., Wang, Y.H., Qu, Y.S., Wei, Q.Y., Li, H.Q., 2018. Effect of the organizational
543 difference of corn stalk on hemicellulose extraction and enzymatic hydrolysis. *Ind.*
544 *Crops Prod.* 112, 698-704.

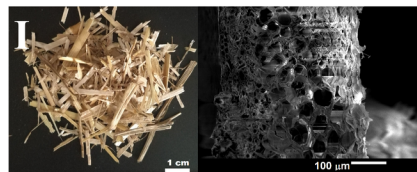
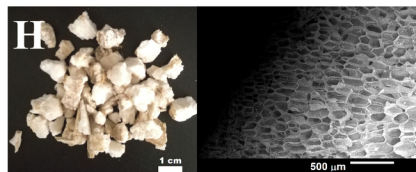
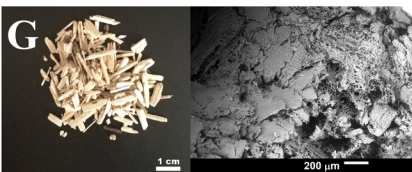
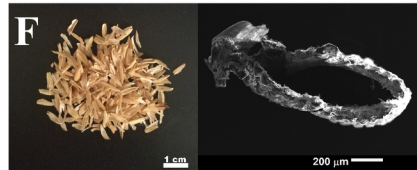
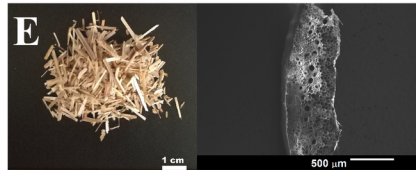
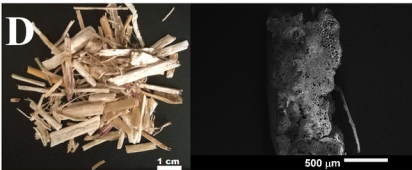
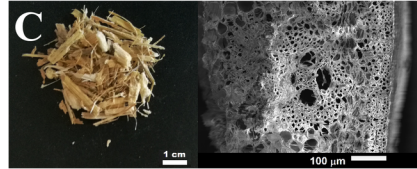
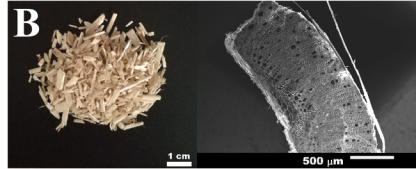
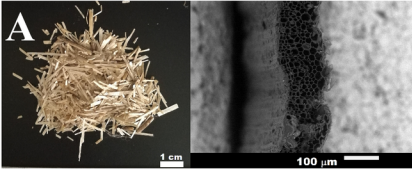
545

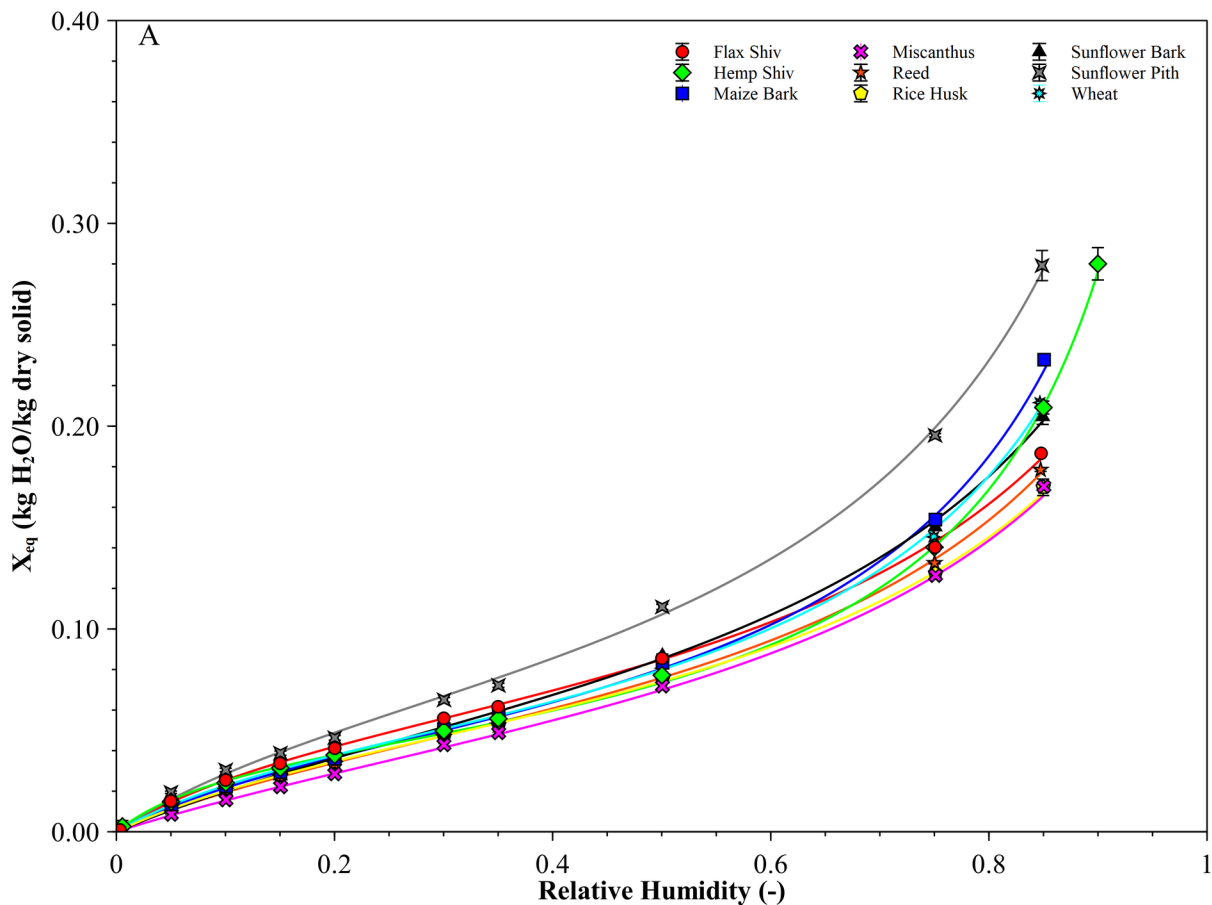
546 **Caption for Figures**

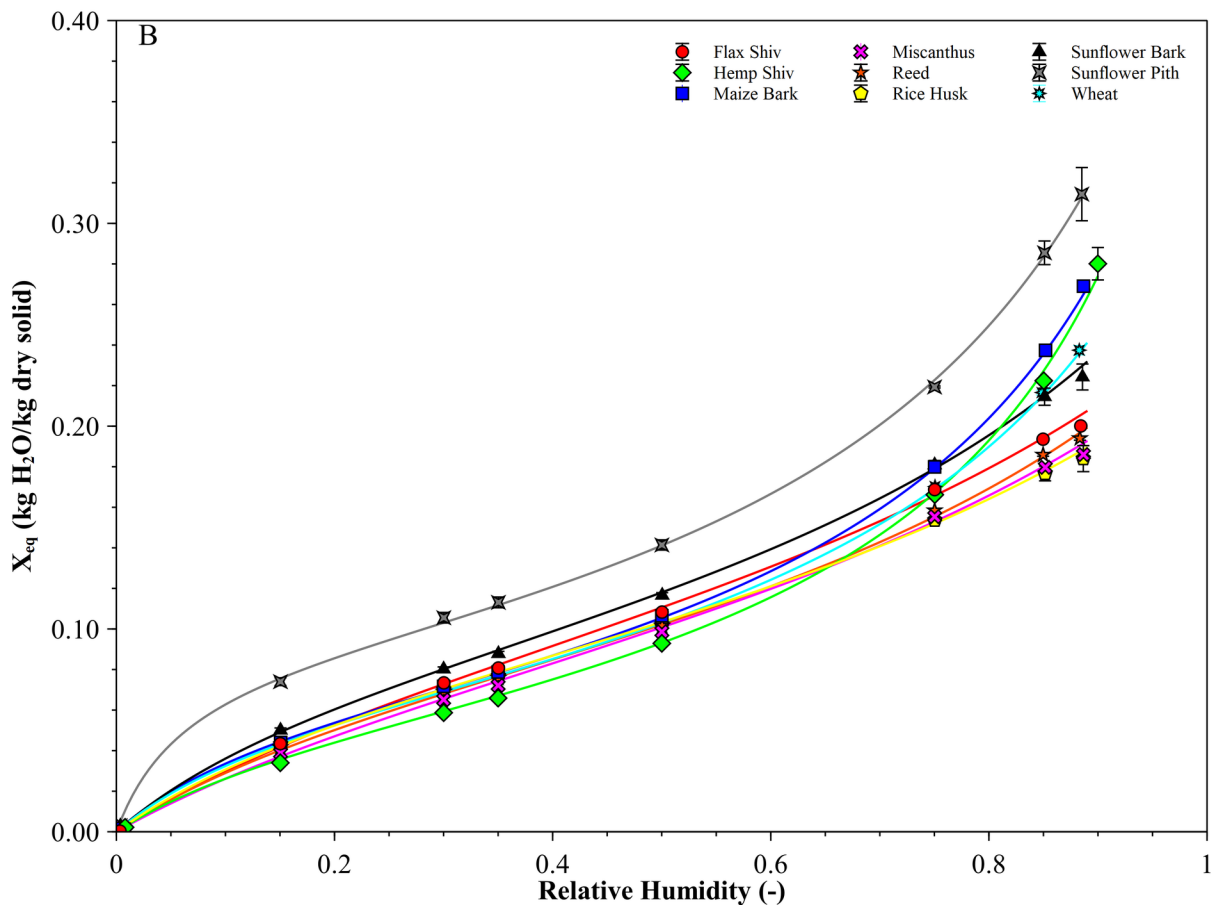
547 **Figure 1.** Images of the studied plant particles. A: Flax Shiv; B: Hemp Shiv; C: Maize Bark;
548 D: Miscanthus; E: Reed; F: Rice Husk; G: Sunflower Bark; H: Sunflower Pith; I: Wheat.

549 **Figure 2.** Water adsorption (A) and desorption (B) isotherms of the studied systems. Line
550 corresponds to GAB model, Eq. (3).

551 **Figure 3.** Water absorption (A) and solid loss kinetics (B) of the studied systems. Line
552 corresponds to Nagy and Vas model, Eq. (9).







W_{A, MF} (kg water/kg final dry solid)

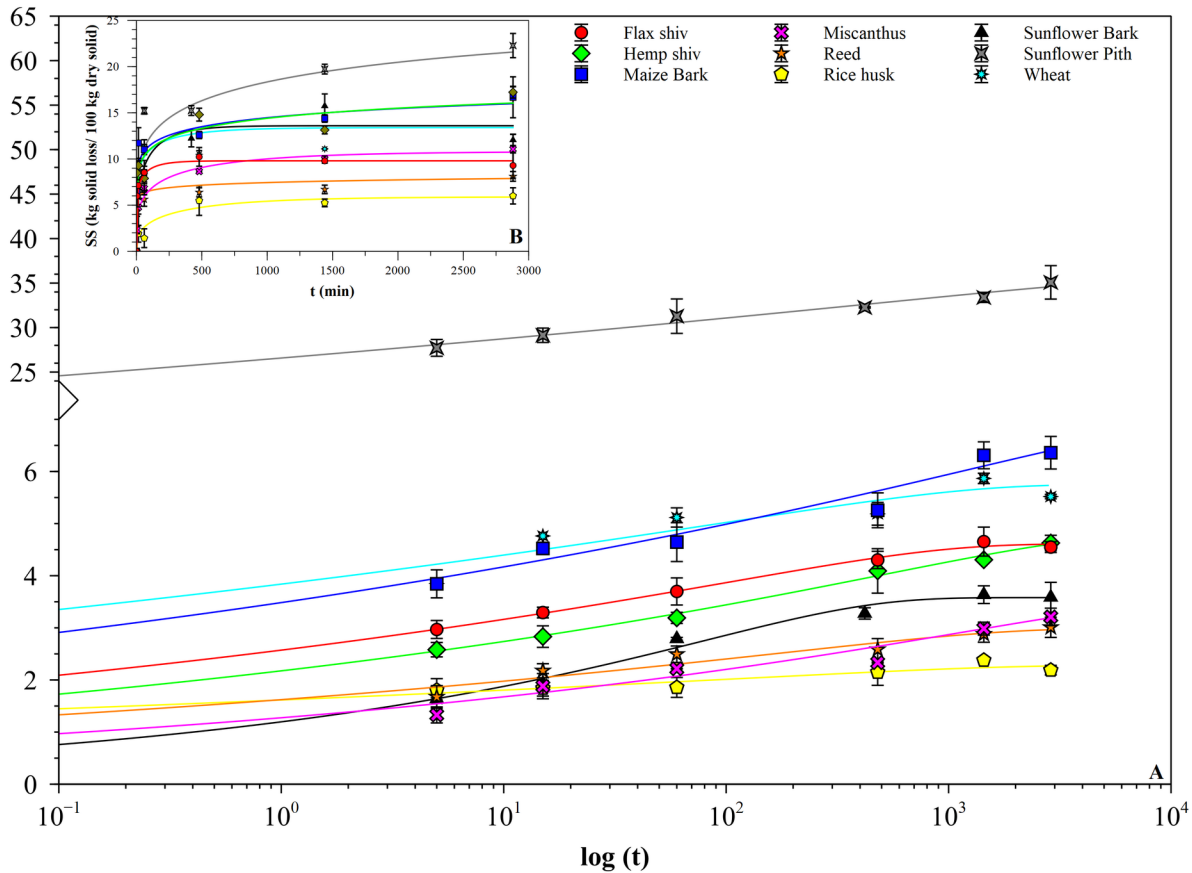


Table 1. Chemical composition of different studied plant particles.

Sample	Soluble (% d.b.)	Hemicellulose (% d.b.)	Cellulose (% d.b.)	Lignin (% d.b.)	Ash (% d.b.)	X_{initial} (% d.b.)
Flax Shiv	9.1±1.9	17.6±2.4	43.5±4.7	27.1±4.5	2.7±0.9	4.7±0.7
Hemp Shiv	17.2±1.1	21.6±1.8	49.0±2.8	8.1±0.6	4.1±1.6	3.1±0.4
Maize Bark	15.3±0.2	34.8±0.9	42.8±1.0	3.3±0.2	3.8±0.2	2.8±0.1
Miscanthus	7.2±0.5	27.8±1.4	43.6±9.8	19.0±10.8	2.4±0.1	3.5±1.5
Reed	9.6±1.5	28.3±1.3	47.6±1.2	10.5±1.5	4.0±0.1	2.4±0.1
Rice Husk	7.7±0.3	19.8±0.5	42.1±0.6	16.8±0.2	13.7±0.1	1.9±0.1
Sunflower Bark	6.0±2.2	18.1±2.8	30.3±6.2	41.7±8.5	3.8±0.5	6.5±0.1
Sunflower Pith	38.6±1.1	5.0±1.9	23.3±6.8	21.4±6.4	11.7±0.3	8.7±0.3
Wheat	10.5±0.1	34.1±4.5	45.3±4.3	6.2±0.3	3.9±0.1	5.5±0.1

% d.b.: g/100 g dry solid; X_{initial}: Humidity of samples before starting the tests.

Table 2. Parameters of Lognormal function, Eq. (1), corresponding to systems length and width frequency distribution, apparent (ρ_A), compacted (ρ_C) and true (ρ_T) densities and open porosity ($\theta=1-\rho_A/\rho_T$), Eq. (2).

Sample	Length				Width				Density (kg/m ³)			Open Porosity (-)
	μ	σ	R ²	E _{RMS} (-)	μ	σ	R ²	E _{RMS} (-)	ρ_B	ρ_C	ρ_T	θ
Flax Shiv	2.070	0.320	0.999	0.008	0.265	0.330	0.999	0.009	101±5	144±4	1406±19	0.928
Hemp Shiv	1.503	0.546	0.999	0.011	0.157	0.565	0.998	0.013	114±4	167±6	1247±41	0.909
Maize Bark	1.633	0.633	0.999	0.010	0.446	0.760	0.999	0.008	67±2	112±3	1075±6	0.938
Miscanthus	1.812	0.829	0.998	0.014	0.288	1.036	0.997	0.015	128±5	186±9	940±9	0.864
Reed	2.057	0.679	0.998	0.017	0.283	0.639	0.997	0.010	81±2	134±3	1016±11	0.920
Rice Husk	2.077	0.129	0.985	0.040	0.840	0.305	0.997	0.015	112±2	147±4	1328±26	0.916
Sunflower Bark	2.373	0.385	0.997	0.017	1.364	0.330	0.999	0.010	157±9	176±6	1395±12	0.887
Sunflower Pith	1.641	0.395	0.998	0.014	1.278	0.400	0.999	0.009	21±3	31±4	754±25	0.973
Wheat	2.233	0.596	0.999	0.011	0.557	0.731	0.993	0.027	45±4	85±5	1163±13	0.961

Table 3. GAB model, (Eq. 3), parameters for water sorption isotherms of studied plant particles.

Agroresource	Adsorption					Desorption					a_s (m ² /g) Eq. (5)
	C (-)	K (-)	X _m (d.b.)	R ² (-)	E _{RMS} (d.b.)	C (-)	K (-)	X _m (d.b.)	R ² (-)	E _{RMS} (d.b.)	
Flax Shiv	7.0±0.1	0.812±0.004	0.061±0.001	0.9995	0.002	5.2±0.4	0.607±0.038	0.111±0.010	0.9994	0.003	178.9±0.6
Hemp Shiv	10.8±1.3	0.941±0.008	0.043±0.001	0.9997	0.002	6.3±1.3	0.863±0.034	0.064±0.007	0.9997	0.002	156.6±8.0
Maize Bark	6.0±0.2	0.919±0.006	0.052±0.001	0.9998	0.002	8.2±0.4	0.834±0.010	0.072±0.002	0.9999	0.001	168.8±0.1
Miscanthus	3.6±0.1	0.805±0.001	0.060±0.001	0.9996	0.002	4.8±0.4	0.612±0.031	0.103±0.008	0.9994	0.003	170.1±1.8
Reed	5.0±0.1	0.829±0.001	0.057±0.001	0.9997	0.001	5.9±0.1	0.660±0.013	0.092±0.002	0.9997	0.002	158.2±1.1
Rice Husk	5.7±0.2	0.817±0.015	0.055±0.001	0.9997	0.001	6.5±0.1	0.618±0.023	0.096±0.003	0.9997	0.002	172.3±2.4
Sunflower Bark	4.1±0.1	0.820±0.009	0.068±0.001	0.9997	0.002	7.0±0.1	0.684±0.003	0.099±0.001	0.9997	0.002	196.9±5.8
Sunflower Pith	5.7±0.1	0.884±0.018	0.073±0.003	0.9997	0.002	20.2±1.1	0.811±0.030	0.090±0.005	0.9998	0.002	205.2±1.6
Wheat	6.7±0.2	0.900±0.002	0.052±0.001	0.9998	0.001	7.8±0.2	0.796±0.004	0.074±0.000	0.9999	0.000	160.8±0.1

d.b.: g water/g dry solid

Table 4. Nagy and Vas model parameter, Eq. (9), for different plant particles.

Parameter	Flax shiv	Hemp shiv	Maize Bark	Miscanthus	Reed	Rice Husk	Sunflower Bark	Sunflower Pith	Wheat
$WA_{F\infty}$ (kg water/ kg d.s.)	4.6	4.8	7.1	3.6	3.0	2.3	3.6	35.8	5.7
A_{WAF}	0.033	0.007	0.003	0.003	0.019	0.032	0.039	0.009	0.036
K_{WAF}	0.089	0.100	0.078	0.119	0.086	0.048	0.197	0.034	0.059
R^2	0.999	0.998	0.991	0.976	0.983	0.989	0.993	0.999	0.983
E_{RMS} (kg water/ kg f.d.s.)	0.1	0.1	0.2	0.2	0.1	0.1	0.1	0.4	0.2
$WA_{0\infty}$ (kg water/ kg i.d.s.)	4.1	3.7	5.8	3.1	2.6	2.1	3.0	29.0	4.9
A_{WA0}	0.027	0.035	0.003	0.003	0.170	0.055	0.051	0.009	0.057
K_{WA0}	0.078	0.110	0.065	0.112	0.187	0.036	0.182	0.012	0.050
R^2	0.999	0.998	0.992	0.982	0.986	0.991	0.988	1.000	0.979
E_{RMS} (kg water/ kg i.d.s.)	0.0	0.1	0.1	0.1	0.1	0.1	0.1	0.4	0.2
SL_{∞} (kg solid/ kg i.d.s.)	9.8	17.9	18.4	10.8	9.1	5.9	13.6	25.4	13.4
A_{SL}	0.124	0.003	0.002	0.011	0.001	0.009	0.034	0.002	0.038
K_{SL}	0.162	0.121	0.104	0.229	0.056	0.332	0.287	0.181	0.143
R^2	0.994	0.927	0.941	0.975	0.960	0.918	0.868	0.940	0.838
E_{RMS} (kg solid/ kg i.d.s.)	0.3	1.4	1.3	0.6	0.5	0.6	1.9	1.9	2.0

kg i.d.s.: kg of initial dry solid; kg f.d.s.: kg of final dry solid